A defining member of the new cysteine-cradle family is a transient aECM protein involved in signalling skin damage

Thomas Sonntag, Shizue Omi, Antonina Andreeva, Nathalie Pujol

A defining member of the new cysteine-cradle family is a transient aECM protein involved in signalling skin damage

Thomas Sonntag[1], Shizue Omi[1], Antonina Andreeva[2], Nathalie Pujol[1]
[1] Aix Marseille Univ, INSERM, CNRS, CIML, Turing Centre for Living Systems, Marseille, France
[2] European Molecular Biology Laboratory, European Bioinformatics Institute (EMBL-EBI), Wellcome Genome Campus, Hinxton, Cambridgeshire CB10 1SD, UK.

Abstract
The apical extracellular matrix acts as crucial barrier, and communicates with the epidermis to trigger protective responses following injury or infection. In *C. elegans*, we previously showed that mutants lacking cuticle furrows exhibit persistent immune activation (PIA). In a genetic suppressor screen, we identified *spia-1* as a key gene downstream of furrow collagens and upstream of immune signaling. *spia-1* expression oscillates during larval development, peaking between each moult together with precuticle and cuticule components. It encodes a secreted precuticular protein that transiently localizes to furrows. It shares a novel cysteine-cradle domain (CCD-aECM) with other aECM proteins, predicted to bind proteins with an exposed hydrophobic α helix. SPIA-1 is proposed to act as a sensor of cuticle damage, mediating immune activation in response to furrow loss and might be part of a checkpoint during the establishment of the new cuticle. This research reinforces the notion of an intricate interplay between cuticle integrity and epidermal immune activation in *C. elegans*.

Introduction

All multicellular organisms must protect themselves from injury and pathogens. *C. elegans* lacks an adaptive immune system and motile immune cells. It relies instead on its epithelial barriers to defend against environmental threats. This makes it a powerful model to address the question of how epithelial cells detect damage. In *C. elegans*, the skin is characterized by a rigid but flexible apical extracellular matrix (aECM), known as the cuticle, that surrounds a single syncytial epidermal layer. The cuticle serves not only as a protective barrier against environmental insults but also as a dynamic interface that communicates crucial signals to the underlying epidermal tissue. We have previously described how cuticle damage sets off a series of responses in the epidermis. These can be triggered by physical injury, infection with the fungus *D. coniospora*, or during the cycling process of moulting. This highlights the organism's ability to mount a protective transcriptional response aimed at maintaining tissue integrity and combating potential threats (Pujol *et al.* 2008a; Ewbank and Pujol 2016; Martineau *et al.* 2021; Aggad *et al.* 2023).

In addition to these stimuli, mutants lacking furrows have emerged as a valuable model for studying the interplay between cuticle integrity and epidermal immune activation. Mutations in any of the six collagens that form periodic furrows in the cuticle (DPY-2, DPY-3, DPY-7, DPY-8, DPY-9, DPY-10) exhibit a persistent immune activation (PIA), similar to the

response triggered by moulting, physical injury or skin infection. Crucially, this immune response involves the activation of the pivotal p38 MAPK/PMK-1 signalling pathway and the downstream SNF-12/SLC6 transporter and STAT-like transcription factor STA-2 (Pujol *et al.* 2008b; Dierking *et al.* 2011; Dodd *et al.* 2018). During infection or injury, the most upstream components known are the Damage Associated Molecular Pattern (DAMP) receptor DCAR-1, a GPCR, and the Gα protein GPA-12 (Zugasti *et al.* 2014). While loss of STA-2 or SNF-12 fully abrogates the induction of an immune response in furrow collagen mutants, inactivation of DCAR-1 only reduces it partially (Zugasti *et al.* 2014). We therefore proposed that a parallel mechanism must link monitoring of furrow collagens to the activation of the immune response in the epidermis.

To gain deeper insights into how cuticle damage is sensed by the epidermis, we conducted a targeted genetic screen to identify genes acting downstream of furrow collagens and upstream of, or in parallel to, GPA-12. It leveraged the observation that worms expressing a gain-of-function form of GPA-12 (GPA-12*) in the adult epidermis exhibit constitutively high levels of antimicrobial peptide (AMP) gene expression ((Ziegler *et al.* 2009); Figure 1A). Notably, one suppressor allele identified in this screen harbours a mutation in the gene *spia-1* (*Suppressor ofPersistent Immune Activation*). This gene encodes a small nematode-specific secreted protein sharing a C-terminal domain with four other *C. elegans* proteins, including DPY-6, a mucin-type protein with a conserved role in cuticle deposition (Sun *et al.* 2022). The structured core of the common C-terminal domain (named CCD-aECM) is formed by evolutionary conserved cysteine interactions and predicted to allow potential homomeric and heteromeric interactions. Our expression and genetic analyses suggest that SPIA-1 functions as a secreted aECM protein, transiently localized to the furrow before each moult, potentially relaying information about the state of the furrow collagens to the underlying epidermis.

Results & Discussion

Identification of *spia-1* as a suppressor of a constitutive immune response

We previously showed that an immune response characterised by the induction of expression of the antimicrobial peptide (AMP) gene *nlp-29* is activated in the *C. elegans* epidermis in response to wounding and infection (Pujol *et al.* 2008a; Zugasti *et al.* 2014; Dodd *et al.* 2018; Taffoni *et al.* 2019; Martineau *et al.* 2021). Interestingly, mutants in furrow collagens, which lack the furrow structure (“furrow-less mutants”) (Essmann *et al.* 2016; Aggad *et al.* 2023), also have a persistent immune activation (PIA) (Pujol *et al.* 2008b; Zugasti *et al.* 2014, 2016), in parallel to constitutively active detoxification and hyperosmotic responses (Dodd *et al.* 2018). The fact that these 3 responses are induced by the absence of furrows, yet differ in their signalling and effectors, led to the suggestion that a cuticle-associated damage sensor coordinates these 3 responses (Dodd *et al.* 2018).

To identify this potential damage sensor, we have run a pilot suppressor screen, designed to identify only the upstream components of the pathway leading to the induction of the immune response in furrowless mutants. The screen relies on the observation that a constitutively active form of GPA-12 (GPA-12*) provokes a PIA by activating the p38/PMK-1 – STA-2 pathway and on the use of a conditional promoter that is only active in the adult epidermis (Lee *et al.* 2018). In addition to a construct expressing GPA-12* uniquely in the adult epidermis, the strain IG1389 that we designed and constructed, has the well-characterised *nlp-29* promoter driving GFP expression (*nlp-29*p::GFP) and a control DsRed transgene

constitutively expressed in the epidermis (Pujol *et al.* 2008a). In this strain, the *nlp-29*p::GFP reporter is not expressed in larvae but only in the adult, due to the expression of GPA-12* (Figure 1A). When any of the six furrow collagen genes, including *dpy-7*, is inactivated by RNAi in this strain, worms exhibit a high level of GFP at all developmental stages (green larvae-green adults) (Figure 1A-B). Inactivating any gene acting downstream of GPA-12, like *pmk-1* or *sta-2*, completely abolishes the expression of *nlp-29*p::GFP at all stages (red larvae-red adults; the so-called Nipi phenotype (Pujol *et al.* 2008a)) (Figure 1B).

We mutagenized the strain IG1389 using EMS, then transferred synchronised F2 progeny onto *dpy-7* RNAi plates at the L1 stage and screened for mutants that suppressed the PIA phenotype at the L3-L4 larval stage. These individuals were then monitored into adulthood. In many alleles, the PIA phenotype was also blocked at the adult stage. Complementation tests allowed us to identify new alleles of components of the known p38 MAPK pathway including *snf-12(fr189)* and *sta-2*, validating our screen. In a subset of mutants, the PIA phenotype that had been suppressed in L3-L4 worms was again apparent in adults, triggered by the activation of GPA-12 (red larvae-green adult). These alleles were potentially the most interesting as they would be expected to affect signalling upstream of, or in parallel to, *gpa-12*. One candidate *fr179* had a very clear phenotype and was further characterized. We called it *spia-1* for *Suppressor of Persistent Immune Activation* (Figure 1B). The *spia-1(fr179)* strain was backcrossed with the premutagenised strain lacking *gpa-12**, relying on the suppression of *nlp-29*p::GFP induction upon *dpy-7* RNAi for the selection of *spia-1(fr179)* progeny. We confirmed that the *fr179* mutation abrogates the PIA phenotype produced by RNAi inactivation of any of the six furrow collagen genes but it does not suppress the associated short size (i.e. the DPY phenotype; Figure 1C). These results define *spia-1(fr179)* as a suppressor of PIA phenotype, acting downstream of furrow collagens and upstream of, or in parallel to, GPA-12.

The underlying molecular lesion was then characterised by mapping through whole genome sequencing (WGS) of a pool of backcrossed *spia-1(fr179)* (Doitsidou *et al.* 2010; Labed *et al.* 2012). The *spia-1(fr179)* worms carry a mutation in a splice donor site of the gene *F09F9.2* (hereafter *spia-1*), predicted to result in a transcript with a frameshift and the introduction of a premature stop codon leading to a truncated protein of 133 aa. To validate that the inactivation of *F09F9.2* was responsible for the suppressive phenotype, we first abrogated *spia-1* by RNAi inactivation in *dpy-7* mutants and showed that it suppressed the constitutive activation of *nlp-29*p::GFP (Figure S1). We then generated by CRISPR a deletion of 710 bp in *spia-1* with a modification of bp 789 (C -> T) to create a premature stop codon, resulting in a truncated SPIA-1 protein of 26 aa (Figure 1E). *spia-1(syb7920)* suppressed the constitutive activation of *nlp-29*p::GFP in a *dpy-7* mutant (Figure 1F). Moreover, the constitutively-induced immune response could be rescued in the *spia-1(fr179)* background with an extra-chromosomal array bearing the *spia-1* gene with 1.2 kb of upstream sequence (Figure 1G). These results together demonstrate unequivocally that *spia-1* is required for the constitutive immune response in furrow-less mutants.

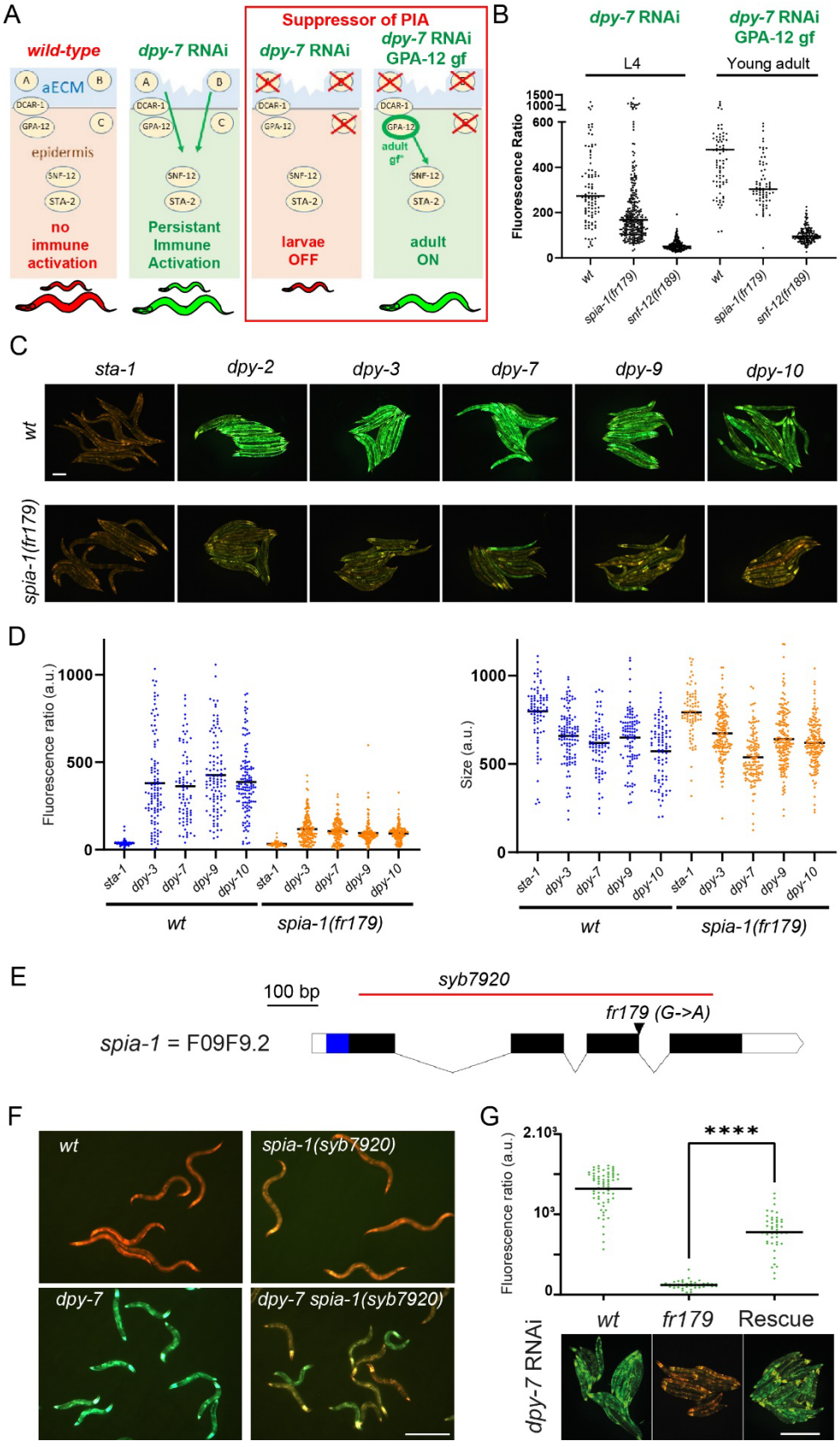

Figure 1. **Mutation in *spia-1* suppresses furrow collagen AMP induction**
(A) Design of the suppressor screen. The strain used has the *frIs7* transgene, i.e both a transcriptional reporter of AMP gene (*nlp-29*p::GFP) and a control DsRed transgene constitutively expressed in the epidermis. Under standard growth conditions, only the control transgene is expressed and worms are red at all stages (left). RNAi inactivation

of any furrow collagen gene, like *dpy-7*, lead to the expression of *nlp-29*p::GFP in a PMK-1/STA-2 dependent manner: worms appear "green" at all stages (middle). The strain we used for the suppressor screen additionally bears the *frIs30* construct to express a gain of function of GPA-12 in the epidermis, only from the young adult stage. In this strain, inactivation of a gene downstream of GPA-12 completely eliminates the expression of *nlp-29*p::GFP in both larvae and adults (Nipi phenotype (Pujol *et al.* 2008a)), whereas inactivation of any gene acting upstream (A) of, or in parallel (B/C) to, GPA-12 inhibits the expression of *nlp-29*p::GFP in the larvae but is rescued by the activation of GPA-12 in the adults (red larvae, green adults, right). Red and green fluorescence were visualized simultaneously in all following images. (B) Quantification of relative green fluorescence in worms carrying *frIs7* with the Biosort: the *frIs30* (green), *spia-1(fr179);frIs30* (orange) and *snf-12(fr189);frIs30* (red) strains upon *dpy-7* RNAi, in L4 and young adults stage (n >70). (C-D) *spia-1(fr179)* suppresses the induction of *nlp-29*p::GFP in young adult worms after RNAi inactivation of furrow collagen genes. *wt* and *spia-1(fr179)* carrying the *frIs7* transgene were treated with the indicated RNAi bacteria, with *sta-1* used as a control (see Mat&Methods). (C) Representative images of young adults, scale bar, 200 µm. (D) Quantification of relative green fluorescence (left panel) and the length of the worms (right panel) with the Biosort (n >70). (E) Structure of the *spia-1* genomic locus. The location of the *fr179* mutation is indicated with an arrowhead, the extent of the *syb7920* deletion is shown with a red line. Exons are shown as black boxes, introns as solid lines. UTR are represented as white boxes, the blue region shows the sequence encoding the signal peptide of *spia-1*. (F) Wild-type or *dpy-7(e88); frIs7* young adults, with or without the *spia-1(syb7920)* deletion. The *spia-1(syb7920)* deletion also suppresses the induction of the *nlp-29*p::GFP transgene in *dpy-7* mutants. (G) The suppression of the immune response in *spia-1* mutants is rescued by the *spia-1* gene. Level of *nlp-29*p::GFP induction following *dpy-7* RNAi is analysed in *wt*, *spia-1*(*fr179)*, and *spia-1(fr179) frEx632[pSO23(spia-1p::spia-1::3UTR spia-1; myo-2p::mCherry]* strains. Top, quantification of the relative green fluorescence with the Biosort (n >40). Bottom, representative images, scale bar, 500 µm.

spia-1 encodes a secreted protein with a novel cysteine-cradle domain

SPIA-1 is predicted to encode a secreted nematode-specific protein of 165 aa with no previously known function (Davis *et al.* 2022). Its C-terminal region is annotated by Panther database with a signature PTHR37435 that has no associated function and identified only in nematodes (Thomas *et al.* 2022; Davis *et al.* 2022). This Panther family includes 5 other secreted *C. elegans* proteins, DPY-6, a mucin-like hydrogel-forming protein (Sun *et al.* 2022) and 4 other uncharacterised nematode specific proteins: F01G10.9, F13B9.2, Y34B4A.10 and F33D4.6 (Figure 2A). These proteins have different lengths and contain regions with a compositional bias suggesting they may be largely intrinsically disordered. Their common and most conserved part is located toward the C-terminus and predicted by AlphaFold2 to adopt a globular structure composed of four α-helices (Jumper *et al.* 2021). The latter are arranged in two nearly orthogonal pairs, with two helices of one pair packed at both edges of the other and thus creating a cradle-shaped domain. This globular domain contains 4 invariant cysteines that define a sequence motif C_1-$(X)^{22}$-C_2-$(X)^7$-P-$(X)^3$-C_3-$(X)^9$-C_4. The cysteine residues are predicted to form two disulfide bonds connecting the α-helices with C_1 bonding C_4 and C_2 bonding C_3 (Figure 2B) (Jumper *et al.* 2021). These disulfide bonds are likely to play a structural role and be essential for the maintenance of the cradle-like shape of the domain. They also support the formation of a highly hydrophobic groove that is probably involved in binding of an unknown interaction partner, or alternatively, in dimerisation (Figure 2C and 2D). Interestingly, in the AlphaFold2 model of Y34B4A.10 (uniprot ID:Q8WSP0), an N-terminal α-helix of the protein itself docks into this groove. The residues that constitute this groove are also semi-conserved suggesting they may be important for function (Figure 2B). Owing to its features, this domain was named 'aECM cysteine-cradle domain' (short name CCD-aECM) and its sequence diversity was added to the Pfam database (Mistry *et al.* 2021) as a new entry PF23626.

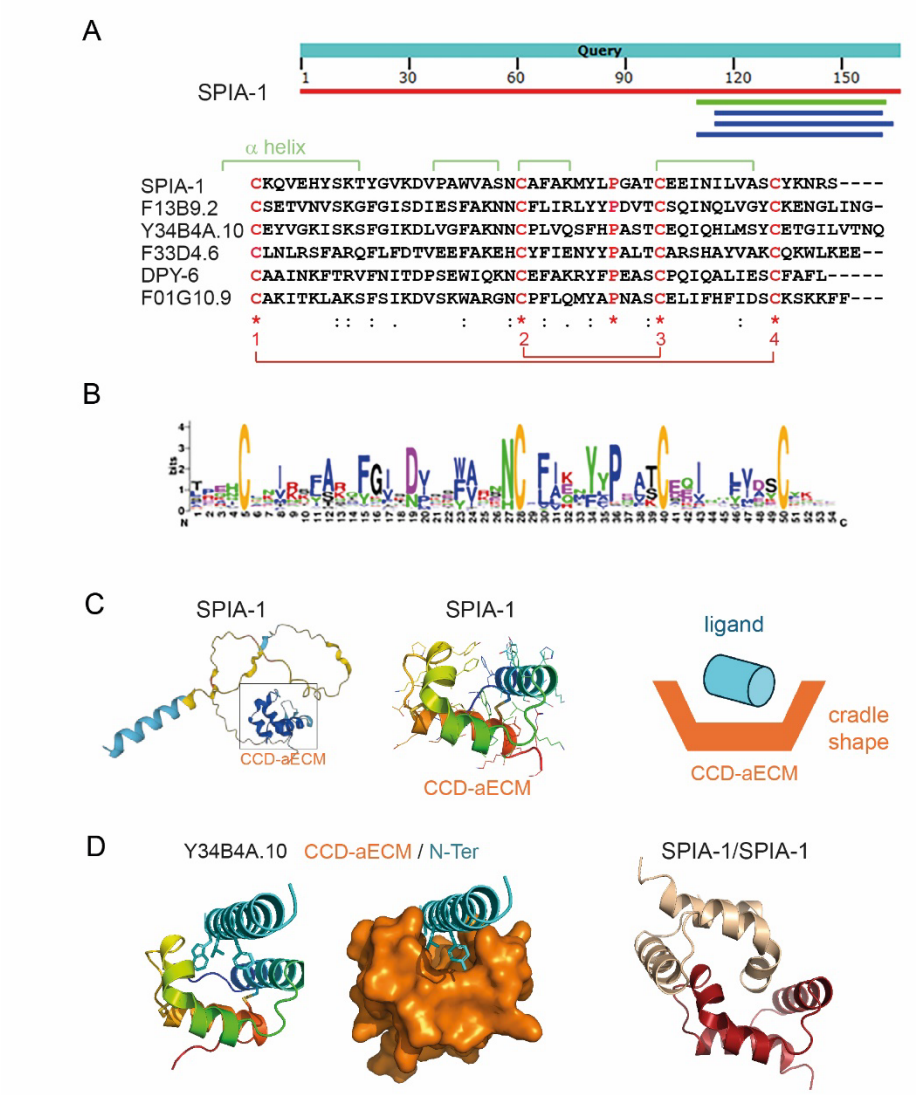

Figure 2. **SPIA-1 is a secreted protein containing a novel cysteine-cradle domain**
(A) Blast search retrieved 5 *C. elegans* proteins that share a common CCD-aECM domain in their C-terminal region. This domain contains 4 invariantly spaced cysteines predicted to form two disulfide bridges. Their formation is likely to stabilise the CCD-aECM domain tertiary structure and to be essential for function. Thus they define the evolutionary most conserved feature of this domain. (B) Homologues of SPIA-1 CCD-aECM domain were identified in nematodes. Sequence logo derived from the Pfam (PF23626) SEED alignment shows residues conserved across nematode homologues, some of which are likely to have a structural role while others may be essential for function. The relative size of the residue letters indicate their frequency in the aligned sequences of the Pfam SEED. (C) AlphaFold2 prediction of the full length SPIA-1 protein, left, and prediction of the CCD-aECM domain of SPIA-1. The SPIA-1 CCD-aECM domain is shown in cartoon colored by rainbow with the side-chains shown as sticks. The cradle-like shape of the domain allows binding of a hydrophobic α helix. (D) The CCD-aECM hydrophobic groove can potentially engage in heteromeric or homomeric interactions. AlphaFold2 prediction of Y34B4A.10 is shown as both cartoon and surface models with the predicted bound N-terminal helix shown in cyan. Residues from this α helix that are predicted to engage in hydrophobic interactions are shown as sticks. AlphaFold2 multimer predicts dimeric SPIA-1 CCD-aECM with an ipTM score ~0.6 (moderate confidence score) in which one of the helices forming the cradle of one molecule docks into the hydrophobic groove of the other.

spia-1 is expressed in the epidermis and its expression oscillates during larval stages

During larval development, moults happen 4 times, every 7–8 hours at a temperature of 25°C. Genome-wide transcriptomic studies have revealed the rhythmic activity of thousands of genes that align with the moulting cycle. A large proportion of the cycling genes have been shown to be expressed in the epidermis and suggested to be required for the formation of the

new cuticle. The transcripts for SPIA-1 and related proteins are part of these rhythmic oscillations, along with those for pre-cuticle and cuticle components and AMPs (Figure 3A) (Meeuse *et al.* 2020, 2023). Interestingly, there is a repeated pattern of oscillations in each cycle, which ends with ecdysis, defining a stereotypical peak phase for each transcript as described previously (Meeuse *et al.* 2020, 2023). Analysing the data from (Meeuse *et al.* 2020, 2023), we observed that one of the first genes to start to oscillate in the early L1 is *dpy-6*. It encodes a protein that in addition to the CCD-aECM, and similarly to mucins, is enriched with tandem repeats of serine and threonine residues that are likely subject to glycosylation; the resulting glycosylation sites when hydrated can form hydrogels. The early function of DPY-6 in cuticle morphogenesis would be interesting to explore further. We analysed the peak phase of genes that are known to be important for cuticle morphogenesis and organised them relative to *dpy-6*. All 5 genes encoding a CCD-aECM domain cycle just after the pre-cuticle genes *let-653* and *fbn-1,* with *F01G10.9* peaking together with the pre-cuticle genes *noah-1/2* & *lpr-3* and the 6 furrow Dpy collagens *dpy-2, dpy-3, dpy-7, dpy-8, dpy-9, dpy-10*, followed by *spia-1, F13B9.2*, *F33D4.6* and *Y34B4A.10*. These are then followed by the non-furrow collagens like *dpy-4, -5, -13*. The cycle is closed by AMPs including *nlp-29* that have been proposed to be induced to protect the epidermis while the old cuticle is shed (Martineau *et al.* 2021) (Figure 3B). The observation that *spia-1* and its paralogues cycle at the beginning of the new cuticle synthesis with precuticle and furrow collagen genes suggest a role in patterning the new cuticle, including a very early role for *dpy-6*.

Targeted DamID (TaDa) studies are consistent with SPIA-1 expression in the syncytial epidermis hyp7 in larval stages (Katsanos *et al.* 2021). In adult-specific single cell RNAseq, *spia-1* is also found expressed in cephalic and inner labial socket and phasmid sheet cells (Ghaddar *et al.* 2023). A transcriptional reporter confirmed that *spia-1* is expressed in the main epidermal cell and socket cells but is not visible in other epithelial cells like the seam cells, nor in the vulval cells (Figure 3C-G). The expression starts in embryos at the 2-fold stage, which is the time when the pre-cuticle starts to be assembled (Figure 3C) (Cohen and Sundaram 2020; Birnbaum *et al.* 2023). The transcriptional reporter might be missing some of the endogenous regulation, but it includes 1.2 kb of upstream genomic sequence that harbors several transcription factors binding motifs, including NHR-23 that is important for oscillatory gene expression in epithelial cells (Gerstein *et al.* 2010; Davis *et al.* 2022; Johnson *et al.* 2023). Taken together these observations suggest that the *spia-1* gene is expressed in epidermal cells; the oscillating expression of *spia-1* during larval development is consistent with a role in cuticle morphogenesis.

Figure 3. ***spia-1* and all CCD-aECM genes are oscillatory expressed between each molt**
(A) AMP and aECM gene expression oscillates between each moult, data from (Meeuse *et al.* 2020). (B) Between each molt, a time line of gene expression is represented, with *dpy-6* starting each cycle, data from (Meeuse *et al.* 2020). (C-G) Expression pattern of *spia-1* transcript in worms carrying the *frEx631[pSO22(spia-1*p::GFP*), myo-2p::mCherry]* transgene. Representative confocal images of (C) 2-fold embryo, (D) L1 larva, (E) adult head, arrow points to the sheath cell, arrowhead to a neurone (F) L4 larva, (G) L4 vulva. Grey color in (G) was acquired with a transmitted detection module; scale bar, 10 µm.

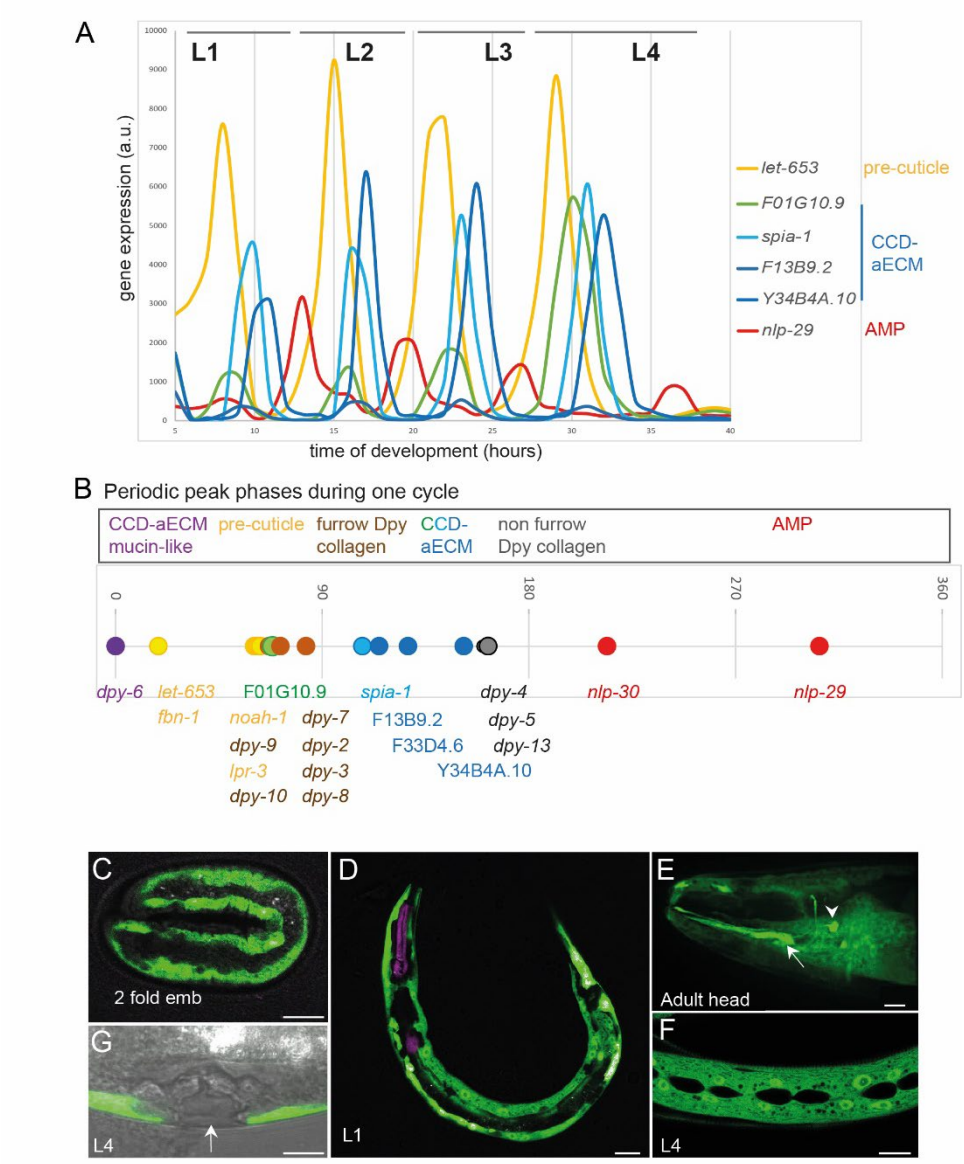

SPIA-1 is transiently localized to aECM periodic furrows

We tagged the SPIA-1 protein by insertion of GFP in 3 different positions, at the N-terminus after the signal peptide, at the C-terminus before the stop codon, or internally before the CCD-aECM. Only the internally tagged SPIA-1::sfGFP behaved as a functional protein, able to rescue the PIA phenotype when expressed transgenically in mutants (Figure 4A). SPIA-1::sfGFP started to be visible in late embryonic stages in association with the furrows and then seemed to be internalised and degraded,reappearing before each moult (Figure 4B). This dynamic behaviour is similar to that exhibited by several precuticular components (Gill *et al.* 2016; Birnbaum *et al.* 2023). We conducted a precise temporal analysis throughout the L4 larval stage, using vulval shape as a proxy for developmental timing (Mok *et al.* 2015), as previously described (Cohen *et al.* 2020; Katz *et al.* 2022; Aggad *et al.* 2023). The precuticular lipocalin LPR-3 was shown to be only transiently present during the L4 stage, being secreted from the L4.3 stage onwards, and observed in an annular pattern between L4.4 to L4.7 (Forman-Rubinsky *et al.* 2017; Katz *et al.* 2022). In a double labelled mCherry::LPR-3, SPIA-1::sfGFP strain, SPIA-1 started to be visible at the L4.4 stage, and in a pattern complementary to LPR-3. Its level then decreased as SPIA-1 and LPR-3 accumulated in vesicles (Figure 4C). In addition, SPIA-1::sfGFP

was found to accumulate in the vulva lumen during the L4 stage, as has been described for other precuticular components that are required for the shaping of the vulva (Cohen *et al.* 2020), even if *spia-1* is not expressed in vulval cells (Figure 4B). Altogether, this suggests that SPIA-1 is an early precuticular component, that together with the hedgehog-related protein GRL-7 (Chiyoda *et al.* 2021; Serra *et al.* 2023), is one of the few known to be specifically positioned at the furrows.

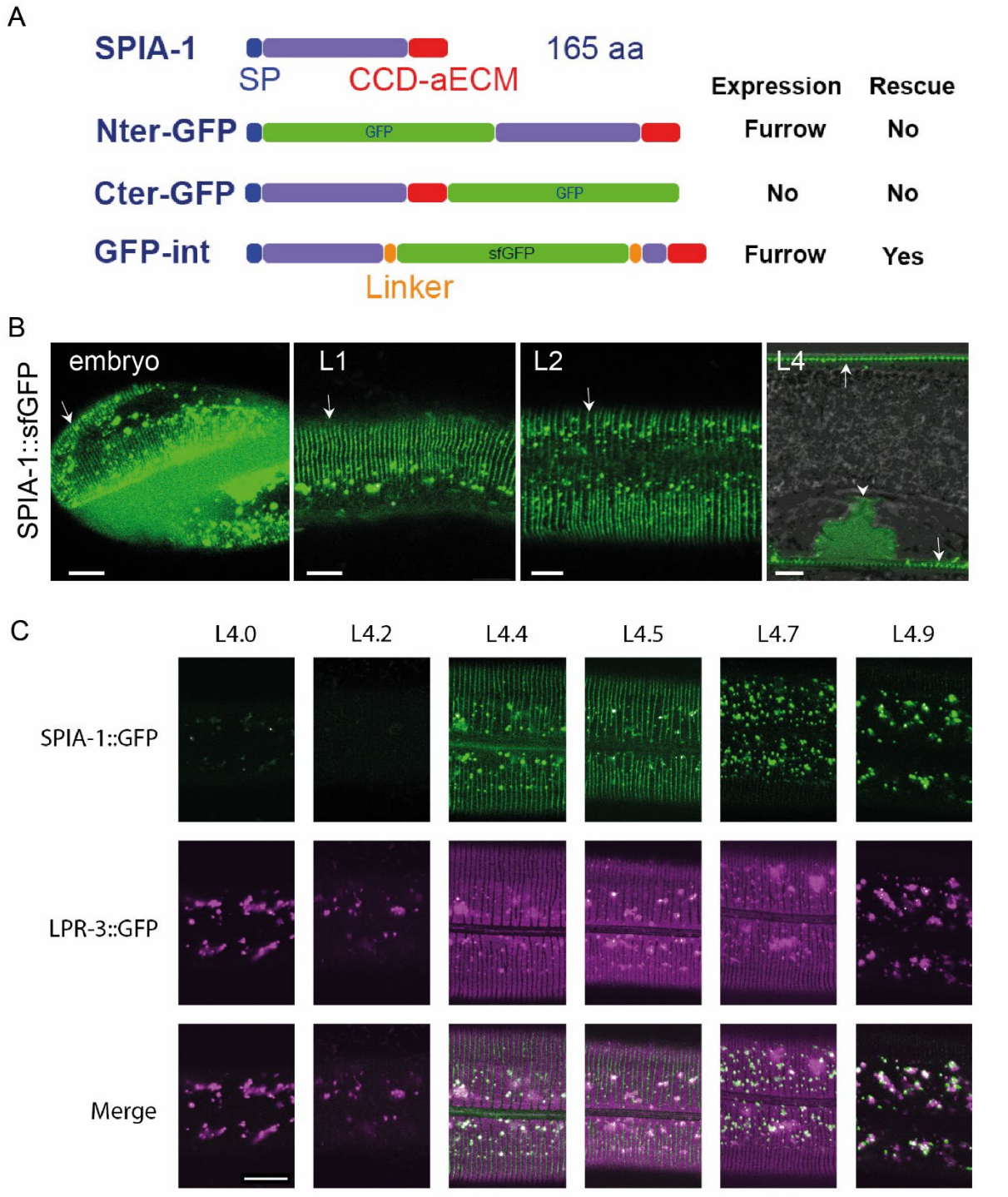

Figure 4. **SPIA-1 is transiently expressed in furrows**
(A) Position of the insertion of GFP in each translational reporter with their expression pattern and rescue activities. (B) Representative confocal images of the SPIA-1::sfGFP reporter (GFP-int) in 3-fold embryo, L1, L2, and L4 vulval lumen. White arrows and arrowhead indicate signal in furrows and in vulval lumen, respectively; scale bar, 5 µm.

(C) The L4 stage is subdivided into sub-stages in relation to the shape of the vulva. SPIA-1::sfGFP and mCherry::LPR-3 are observed in parallel; scale bar, 10 µm.

SPIA-1 acts downstream of collagen furrows

spia-1 was identified as a suppressor of the permanent immune activation provoked by the absence of furrows. As it conceivably exerted its suppressive function by restoring normal furrow morphology, we examined the cuticle of worms deficient for different furrow collagens in the *spia-1(fr179)* background, with a COL-19::GFP marker and a DPY-7::sfGFP marker. In no case did the *spia-1* mutation restore furrows (Figure 5A&B). We noticed that when furrows are absent in a *dpy-7* mutant, the precuticle component LPR-3 cannot assemble anymore in its specific anti-furrow pattern during the mid L4, as visualised with sfGFP::LPR-3. The absence of *spia-1* could not restore the correct LPR-3 localisation (Figure 5C). In a *dpy-7* mutant, the localisation of SPIA-1::sfGFP at the furrow was lost and the pattern observed from L4.4 to L4.7 stage ressembles the one seen in wild-type at the L4.7 stage with small vesicles, but with an overall weaker signal (Figure 5D). This suggest that furrows are required to pattern precuticle components including SPIA-1.

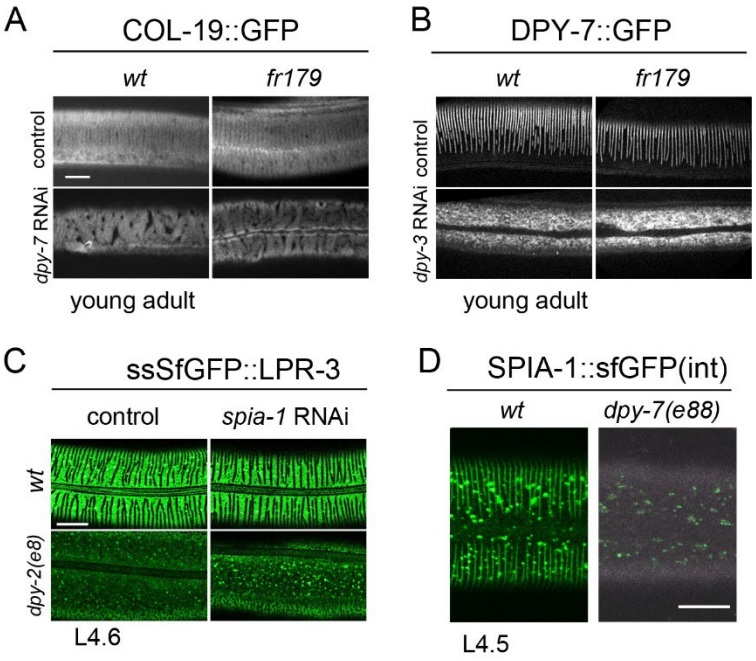

Figure 5. ***spia-1* does not suppress the absence of furrow or precuticle patterning in furrow mutants**
(A) *spia-1(fr179)* does not suppress COL-19::GFP abnormal pattern following *dpy-7* RNAi; representative images of *wt* or *spia-1(fr179)* young adults carrying COL-19::GFP treated with *sta-1* or *dpy-7* RNAi bacteria; scale bar, 10 µm. (B) *spia-1* does not suppress the absence of furrows following *dpy-3* RNAi; representative images of *wt* or *spia-1(fr179)* worms carrying DPY-7::sfGFP treated with *sta-1* or *dpy-3* RNAi bacteria; scale bar, 10 µm. (C) *spia-1* does not suppress the abnormal sfGFP::LPR-3 in *dpy-2(e8)*; representative images of *wt* or *dpy-2(e8)* L4 worms carrying sfGFP::LPR-3 treated with control (*sta-1)* or *spia-1* RNAi bacteria; scale bar, 10 µm. (D) SPIA-1::sfGFP is not found in furrows in *dpy-7* mutants; representative images of *wt* or *dpy-7(e88)* L4.5 worms carrying SPIA-1::sfGFP; scale bar, 10 µm.

SPIA-1 as a sensor of cuticle damage

Our results indicate that SPIA-1 is a specific furrow precuticle component that relies on furrow collagens for its proper localisation. It is required to mediate the immune activation in the epidermis in response to furrow-loss, acting downstream of the furrow collagens. The cradle-shape of the CCD-aECM domain is predicted to engage in protein-protein interactions.

We propose that SPIA-1 could potentially act as part of a meshwork of proteins capable of interacting homo- or heterotypically depending on the available of their respective binding partners, to signal to the epidermis an incorrect patterning of the new cuticle at each larval stage.

Materials and Methods

EMS suppressor screen and mutation identification.

P0 from the strain IG1389 *frIs7[nlp-29*p::GFP*, col-12p::DsRed] IV; frIs30[(col-19p::GPA-12gf), pNP21(pBunc-53::GFP)]* were mutagenized with EMS as previously described (Pujol *et al.* 2008a; Labed *et al.* 2012). Individual synchronised F2 L1 worms were plated on *dpy-7* RNAi plates. Late larval F2 that showed a low expression of *nlp-29*p::GFP were cloned. The ones that then showed a higher GFP expression at adult stage were further analysed. As a positive control for the mutagenesis, several candidates that still abrogate the GFP signal at the adult stage were also cloned, and led to the isolation of several new Nipi alleles including *snf-12(fr189)*. *spia-1* was further backcrossed with IG274 *frIs7[col-12p::DsRed, nlp-29*p::GFP*]* and a dozen of F2 without the GPA-12gf were isolated, then pooled to send their genome to sequencing (BGI). Sequences were analysed with MiModD v0.1.9 and the sub-commands *varcall*, then *varextract* and finally *annotate*. This later step required SnpEff v5 and the SnpEff database *WBcel235.86*. The VCF file produced was re-formatted using a Python script to allow a curation of all putative mutations with user-defined thresholds.

Nematode strains

All *C. elegans* strains were maintained on nematode growth medium (NGM) and fed with *E. coli* OP50, as described (Stiernagle, 2006), the wild-type N2, IG274 *frIs7[col-12p::DsRed, nlp-29*p::GFP*]* IV *fln-2(ot611)* X (Pujol *et al.* 2008a), IG2160 *frIs7[col-12p::DsRed, nlp-29*p::GFP*] IV* IG1389 *frIs7[nlp-29*p::GFP*, col-12p::DsRed] IV; frIs30[(col-19p::GPA-12gf), pNP21(pBunc-53::GFP)],* IG1890 *spia-1(fr179); frIs7[nlp-29*p::GFP*, col-12p::DsRed] IV; frIs30[(col-19p::GPA-12gf), pNP21(pBunc-53::GFP)] I* (Lee *et al.* 2018)*,* IG1890 *spia-1(fr179); frIs7[nlp-29*p::GFP*, col-12p::DsRed] IV; frIs30[(col-19p::GPA-12gf), pNP21(pBunc-53::GFP)] I*, IG2114 *spia-1(fr179); frIs7[nlp-29*p::GFP*, col-12p::DsRed] IV*, IG1997 *spia-1(fr179); frIs7[nlp-29*p::GFP*, col-12p::DsRed] IV; frEx632[pSO23(spia-1p::spia-1::3UTRspia-1; myo-2p::mCherry],* IG2093 *spia-1(fr179) X*, IG2092 *spia-1(fr179) X; dpy-2(e8) II*, PHX7920 *spia-1(syb7920) X* IG2175 *spia-1(syb7920) X; frIs7[nlp-29*p::GFP*, col-12p::DsRed] IV,* IG2177 *dpy-7(e88) spia-1(syb7920) X; frIs7[nlp-29*p::GFP*, col-12p::DsRed] IV,* IG1689 *dpy-7(e88) X; frIs7[nlp-29*p::GFP*, col-12p::DsRed] IV* (Dodd *et al.* 2018)*,* IG2163 *dpy-7(e88) X; frEx649[pSO26(spia-1::sfGFP(int)::3UTR_spia-1), myo-2p::mCherry, rps-0p::HygR]*, IG1988 *frEx631[pSO22(spia-1*p::GFP*), myo-2p::mCherry]*, IG1986 *frEx629[pSO22(spia-1*p::GFP*; ttx-3p::RFP]*, IG2158 *spia-1(fr179) lpr-3(cs266[mCherry::LPR-3]) X; frEx649[pSO26(spia-1::sfGFP(int)::3UTR_spia-1), myo-2p::mCherry, rps-0p::HygR],* IG1999 *frEx633[pSO24(spia-1::GFP::3UTR_spia-1); myo-2p::mCherry],* IG2073 *spia-1(fr179); frIs7[nlp-29*p::GFP*, col-12p::DsRed] IV; frEx633[pSO24(spia-1::GFP::3UTR_spia-1); myo-2p::mCherry], myo-2p::mCherry, rps-0p::HygR],* IG2062 *frEx644[pSO25(spia-1p::signalP::GFP::spia-1::3UTR_spia-1), myo-2p::mCherry, rps-0p::HygR]*, IG2069 *spia-1(fr179); frIs7[nlp-29*p::GFP*, col-12p::DsRed] IV; frEx644[pSO25(spia-1p::signalP::GFP::spia-1::3UTR_spia-1), myo-2p::mCherry, rps-0p::HygR],* IG2108 *spia-1(fr179) X; frEx648[pSO26(spia-1::sfGFP(int)::3UTR_spia-1), myo-2p::mCherry, rps-0p::HygR],* IG2167 *spia-1(fr179) X; frEx649[pSO26(spia-1::sfGFP(int)::3UTR_spia-1), myo-*

2p::mCherry, rps-0p::HygR], IG2112 *spia-1(fr179) X; frIs7[nlp-29*p::GFP*, col-12p::DsRed] IV; Ex648[pSO26(spia-1::sfGFP(int)::3UTR_spia-1), myo-2p::mCherry, rps-0p::HygR],* XW18042 *qxSi722[dpy-7p::DPY-7::sfGFP] II* (Miao *et al.* 2020), IG2071 *spia-1(fr179) X; qxSi722[dpy-7p::DPY-7::sfGFP; ttTi5605] II,* TP12 *kaIs12[COL-19::GFP]* (Thein *et al.* 2003), IG2072 *spia-1(fr179) X; kaIs12[COL-19::GFP]*, UP3666 *lpr-3(cs250[ssSfGFP::LPR-3]) X* & UP3808 *lpr-3(cs266[mCherry::LPR-3]) X* (Forman-Rubinsky *et al.* 2017), IG2166 *lpr-3(cs266[mCherry::LPR-3]) X; frEx649[pSO26(spia-1::sfGFP(int)::3UTR_spia-1), myo-2p::mCherry, rps-0p::HygR]*, IG2158 *spia-1(fr179) lpr-3(cs266[mCherry::LPR-3]) X; frEx649[pSO26(spia-1::sfGFP(int)::3UTR_spia-1), myo-2p::mCherry, rps-0p::HygR],* BE93 *dpy-2(e8) II* (Cox *et al.* 1980), IG2116 *dpy-2(e8) II; lpr-3(cs250[ssSfGFP::LPR-3]) X.*

Constructs and transgenic lines

All constructs were made using SLiCE (Motohashi 2015), all primer sequences used to generated specific PCR amplicons are in Table S1. A rescuing construct (pSO23) was generated by cloning a PCR amplicon (3319-3320) containing the promoter region of *spia-1* (1.23 kb upstream from the start ATG) and the entire genomic region into the pGEMT vector (Promega). A transcriptional construct (pSO22), was generated by cloning a PCR amplicon (3321-3322) containing 1.23 kb upstream of the *spia-1* start codon into pPD95.75 (Fire *et al.* 1990). To create translational constructs, GFP was inserted in *spia-1* either at the C-ter ends (pSO24: 3326-3327) or after N-ter signal peptide (pSO25: 3366-3367, 2093-3365). Internal tag translational construct (pSO26) was generated by inserting the sfGFP (kindly provided by A. Golden and H. Smith) in SPIA-1 at position 92 flanked with N-tag and C-tag linker used in pMLS288 and pMLS287 respectively (Schwartz and Jorgensen 2016) (3392-3393, 3394-3395).

pSO23 was injected at the concentration of 2 ng/µl and the coinjection marker myo-2p::mCherry at 2 ng/µl with the plasmid pKS at 100 ng/µl into IG1954 (*spia-1(fr179); frIs7*) to generate IG1997. pSO22 was injected at the concentration of 50 ng/µl with the coinjection marker ttx-3p::RFP at 50 ng/µl into N2 to get IG1986 and the coinjection marker myo-2p::mCherry at 2 ng/µl into N2 to get IG1988. Translational constructs (pSO24, pSO25, or pSO26) were injected at the concentration of 2 ng/µl, with the coinjection marker myo-2p::mCherry at 2 ng/µl and the hygR selection plasmid pZX13 at 50 ng/µl with pKS at 50 ng/µl into N2 (pSO24 and pSO25), or IG2093 *spia-1(fr179)* (pSO26) to get IG1999, IG2062, IG2108 respectively.

The strain PHX7920 *spia-1(syb7920)* generated by CRISPR editing (SunyBiotech), has a deletion of 710 bp (bp 79-788) in *spia-1* and a modification of bp 78 (C -> **T**) to create a premature stop codon. The sequence from the **ATG** to the original **stop** codon is ATGAAGCTAGTTGTTGTTTTGGCTTGTCTTGTTGTAGTAGCTGAGGCTTATTCAAAATCTGGAAATCCA TACAAGACT**T**AACTTGTGAGGAGATTAACATTTTGGTGGCCTCTTGCTACAAGAACAGAAGC**TAA**, resulting in a truncated SPIA-1 protein of 26 aa. All the transgenic strains carrying *spia-1(fr179)* or *spia-1(syb7920)* were obtained by conventional crosses and genotypes were confirmed by sequencing (see Table S1 for a list of all strains).

Sequence analyses

The following SPIA-1 paralogues (Wormbase geneID/UniProt ID) SPIA-1/Q19281, Y34B4A.10/Q8WSP0, F33D4.6/O44189 (long isoform with the CCD-aECM), DPY-6/Q94185, F01G10.9/O17767 and F13B9.2/Q19385, were analysed with BlastP (Altschul *et al.* 1990), WORMBASE (Davis *et al.* 2022), Panther (Thomas *et al.* 2022), Pfam (Mistry *et al.* 2021) and AlphaFold2 (Jumper *et al.* 2021). We built the Pfam family PF23626 (named 'aECM cysteine-

cradle domain') using sequences of SPIA-1 paralogues with domain boundaries defined based on the AlphaFold2 prediction models. We iteratively searched for homologues using HMMER package and used inclusion threshold of 27 bits. The model of the dimeric SPIA-1 CCD-aECM was generated using AlphaFold2 multimer version 2.3.1, using amber relaxation and no template.

RNA interference

RNAi bacterial clones were obtained from the Ahringer library (Kamath *et al.* 2003) and verified by sequencing (see Table S1). RNAi bacteria were seeded on NGM plates supplemented with 100 g/ml ampicillin and 1 mM Isopropyl-β-D-thiogalactopyranoside (IPTG). Worms were transferred onto RNAi plates as L1 larvae and cultured at 25 °C until L4 or young adult stage. In all our experiments, we are using *sta-1* as our control, as we have shown over the last decade that it does not affect the development nor any stress or innate response in the epidermis (Dierking *et al.* 2011; Zugasti *et al.* 2014, 2016; Lee *et al.* 2018; Zhang *et al.* 2020; Taffoni *et al.* 2020).

Fluorescent reporter analyses

Analysis of *nlp-29*p::GFP expression was quantified with the COPAS Biosort (Union Biometrica; Holliston, MA) as described in (Labed *et al.* 2012). In each case, the results are representative of at least three independent experiments with more than 70 worms analysed. The ratio between GFP intensity and size (time of flight; TOF) is represented in arbitrary units. Representative fluorescent images were taken of transgenic worms mounted on a 2 % agarose pad on a glass slide and anesthetized with 1 mM levamisole in 50 mM NaCl, using the Zeiss AxioCam HR digital colour camera and AxioVision Rel. 4.6 software (Carl Zeiss AG).

Other fluorescent images were acquired using a confocal laser scanning microscope Zeiss LSM780 and its acquisition software Zen with a Plan-Apochromat 40×/1.4 or 63×/1.40 oil DIC M27 objective, or with an inverted Visitron Systems GmbH spinning disk with a Nikon 40×/1.3 oil objective or Zeiss AxioCam HR digital colour camera and Axio Vision Rel. 4.6 software (Carl Zeiss AG).

Acknowledgments

We thank Damien Courtine for the installation and use of MidMod, Ebrima Bojang and Sarah Sharkaoui for participation in the genetic screen that identified *spia-1*. Worm sorting was performed by Jerome Belougne using the facilities of the French National Functional Genomics platform, supported by the GIS IBiSA and Labex INFORM. Some *C. elegans* strains were provided by the CGC, which is funded by NIH Office of Research Infrastructure Programs (P40 OD010440). We thank Andy Golden and Harold Smith for sending us the sfGFP plasmid. The Fire Lab *C. elegans* Vector Kit was a gift from Andrew Fire (Addgene kit # 1000000001). We thank Tim Schedl and the staff at Wormbase for amazing community work including maintenance of a curated database, Meera Sundaram, Jonathan Ewbank and members of the Pujol lab for discussions and comments on the manuscript. We acknowledge the PICsL-FBI photonic microscopy facility of the CIML (ImagImm) from the national infrastructure France-BioImaging supported by the French National Research Agency (ANR-10-INBS-04).

Funding

The project leading to this publication has received funding from the French National Research Agency ANR-22-CE13-0037-01, ANR-10-INBS-04-01 (France Bio Imaging) and France 2030, the

French Government program managed by the French National Research Agency (ANR-16-CONV-0001) and from Excellence Initiative of Aix-Marseille University - A*MIDEX and institutional grants from CNRS, Aix Marseille University. AA is funded by Biotechnology and Biological Sciences Research Council and the NSF Directorate for Biological Sciences (BB/X012492/1).

References

Aggad D., N. Brouilly, S. Omi, C. L. Essmann, B. Dehapiot, *et al.*, 2023 Meisosomes, folded membrane microdomains between the apical extracellular matrix and epidermis. Elife 12: e75906. https://doi.org/10.7554/eLife.75906

Altschul S. F., W. Gish, W. Miller, E. W. Myers, and D. J. Lipman, 1990 Basic local alignment search tool. J Mol Biol 215: 403–410. https://doi.org/10.1016/S0022-2836(05)80360-2

Birnbaum S. K., J. D. Cohen, A. Belfi, J. I. Murray, J. R. G. Adams, *et al.*, 2023 The proprotein convertase BLI-4 promotes collagen secretion prior to assembly of the *C. elegans* cuticle. PLoS Genet 19: e1010944. https://doi.org/10.1371/journal.pgen.1010944

Chiyoda H., M. Kume, C. C. Del Castillo, K. Kontani, A. Spang, *et al.*, 2021 *C. elegans* PTR/PTCHD PTR-18 promotes the clearance of extracellular hedgehog-related protein via endocytosis. PLoS Genet 17: e1009457. https://doi.org/10.1371/journal.pgen.1009457

Cohen J. D., A. P. Sparacio, A. C. Belfi, R. Forman-Rubinsky, D. H. Hall, *et al.*, 2020 A multi-layered and dynamic apical extracellular matrix shapes the vulva lumen in *C. elegans*. Elife 9: e57874. https://doi.org/10.7554/eLife.57874

Cohen J. D., and M. V. Sundaram, 2020 *C. elegans* Apical Extracellular Matrices Shape Epithelia. J Dev Biol 8: E23. https://doi.org/10.3390/jdb8040023

Cox G. N., J. S. Laufer, M. Kusch, and R. S. Edgar, 1980 Genetic and Phenotypic Characterization of Roller Mutants of *C. elegans*. Genetics 95: 317–339. https://doi.org/10.1093/genetics/95.2.317

Davis P., M. Zarowiecki, V. Arnaboldi, A. Becerra, S. Cain, *et al.*, 2022 WormBase in 2022-data, processes, and tools for analyzing *C. elegans*. Genetics 220: iyac003. https://doi.org/10.1093/genetics/iyac003

Dierking K., J. Polanowska, S. Omi, I. Engelmann, M. Gut, *et al.*, 2011 Unusual regulation of a STAT protein by an SLC6 family transporter in *C. elegans* epidermal innate immunity. Cell Host Microbe 9: 425–35. https://doi.org/10.1016/j.chom.2011.04.011.

Dodd W., L. Tang, J. C. Lone, K. Wimberly, C. W. Wu, *et al.*, 2018 A Damage Sensor Associated with the Cuticle Coordinates Three Core Environmental Stress Responses in *C. elegans*. Genetics 208: 1467–1482. https://doi.org/10.1534/genetics.118.300827

Doitsidou M., R. J. Poole, S. Sarin, H. Bigelow, and O. Hobert, 2010 *C. elegans* mutant identification with a one-step whole-genome-sequencing and SNP mapping strategy. PLoS One 5: e15435. https://doi.org/10.1371/journal.pone.0015435

Essmann C. L., M. Elmi, M. Shaw, G. M. Anand, V. M. Pawar, *et al.*, 2016 In-vivo high resolution AFM topographic imaging of *C. elegans* reveals previously unreported surface structures of cuticle mutants. Nanomedicine. https://doi.org/10.1016/j.nano.2016.09.006

Ewbank J. J., and N. Pujol, 2016 Local and long-range activation of innate immunity by infection and damage in *C. elegans*. Curr Opin Immunol 38: 1–7. https://doi.org/10.1016/j.coi.2015.09.005

Fire A., S. W. Harrison, and D. Dixon, 1990 A modular set of lacZ fusion vectors for studying gene expression in *C. elegans*. Gene 93: 189–198. https://doi.org/10.1016/0378-1119(90)90224-f

Forman-Rubinsky R., J. D. Cohen, and M. V. Sundaram, 2017 Lipocalins Are Required for Apical Extracellular Matrix Organization and Remodeling in *C. elegans*. Genetics 207: 625–642. https://doi.org/10.1534/genetics.117.300207

Gerstein M. B., Z. J. Lu, E. L. Van Nostrand, C. Cheng, B. I. Arshinoff, *et al.*, 2010 Integrative analysis of the *C. elegans* genome by the modENCODE project. Science 330: 1775–1787. https://doi.org/10.1126/science.1196914

Ghaddar A., E. Armingol, C. Huynh, L. Gevirtzman, N. E. Lewis, *et al.*, 2023 Whole-body gene expression atlas of an adult metazoan. Science Advances 9: eadg0506. https://doi.org/10.1126/sciadv.adg0506

Gill H. K., J. D. Cohen, J. Ayala-Figueroa, R. Forman-Rubinsky, C. Poggioli, *et al.*, 2016 Integrity of Narrow Epithelial Tubes in the *C. elegans* Excretory System Requires a Transient Luminal Matrix. PLoS Genet 12: e1006205. https://doi.org/10.1371/journal.pgen.1006205

Johnson L. C., A. A. Vo, J. C. Clancy, K. M. Myles, M. Pooranachithra, *et al.*, 2023 NHR-23 activity is necessary for *C. elegans* developmental progression and apical extracellular matrix structure and function. Development 150: dev201085. https://doi.org/10.1242/dev.201085

Jumper J., R. Evans, A. Pritzel, T. Green, M. Figurnov, *et al.*, 2021 Highly accurate protein structure prediction with AlphaFold. Nature 596: 583–589. https://doi.org/10.1038/s41586-021-03819-2

Kamath R. S., A. G. Fraser, Y. Dong, G. Poulin, R. Durbin, *et al.*, 2003 Systematic functional analysis of the *C. elegans* genome using RNAi. Nature 421: 231–237. https://doi.org/10.1038/nature01278

Katsanos D., M. Ferrando-Marco, I. Razzaq, G. Aughey, T. D. Southall, *et al.*, 2021 Gene expression profiling of epidermal cell types in *C. elegans* using Targeted DamID. Development 148: dev199452. https://doi.org/10.1242/dev.199452

Katz S. S., T. J. Barker, H. M. Maul-Newby, A. P. Sparacio, K. C. Q. Nguyen, *et al.*, 2022 A transient apical extracellular matrix relays cytoskeletal patterns to shape permanent acellular ridges on the surface of adult *C. elegans*. PLoS Genet 18: e1010348. https://doi.org/10.1371/journal.pgen.1010348

Labed S. A., S. Omi, M. Gut, J. J. Ewbank, and N. Pujol, 2012 The pseudokinase NIPI-4 is a novel regulator of antimicrobial peptide gene expression. PLoS One 7: e33887. https://doi.org/10.1371/journal.pone.0033887

Lee S. H., S. Omi, N. Thakur, C. Taffoni, J. Belougne, *et al.*, 2018 Modulatory upregulation of an insulin peptide gene by different pathogens in *C. elegans*. Virulence 9: 648–658. https://doi.org/10.1080/21505594.2018.1433969

Martineau C. N., N. V. Kirienko, and N. Pujol, 2021 Innate immunity in *C. elegans*. Curr Top Dev Biol 144: 309–351. https://doi.org/10.1016/bs.ctdb.2020.1

Meeuse M. W., Y. P. Hauser, L. J. Morales Moya, G.-J. Hendriks, J. Eglinger, *et al.*, 2020 Developmental function and state transitions of a gene expression oscillator in *C. elegans*. Mol Syst Biol 16: e9498. https://doi.org/10.15252/msb.20209498

Meeuse M. W. M., Y. P. Hauser, S. Nahar, A. A. T. Smith, K. Braun, *et al.*, 2023 *C. elegans* molting requires rhythmic accumulation of the Grainyhead/LSF transcription factor GRH-1. EMBO J 42: e111895. https://doi.org/10.15252/embj.2022111895

Miao R., M. Li, Q. Zhang, C. Yang, and X. Wang, 2020 An ECM-to-Nucleus Signaling Pathway Activates Lysosomes for *C. elegans* Larval Development. Dev Cell 52: 21-37.e5. https://doi.org/10.1016/j.devcel.2019.10.020

Mistry J., S. Chuguransky, L. Williams, M. Qureshi, G. A. Salazar, *et al.*, 2021 Pfam: The protein families database in 2021. Nucleic Acids Res 49: D412–D419. https://doi.org/10.1093/nar/gkaa913

Mok D. Z. L., P. W. Sternberg, and T. Inoue, 2015 Morphologically defined sub-stages of *C. elegans* vulval development in the fourth larval stage. BMC Dev Biol 15: 26. https://doi.org/10.1186/s12861-015-0076-7

Motohashi K., 2015 A simple and efficient seamless DNA cloning method using SLiCE from Escherichia coli laboratory strains and its application to SLiP site-directed mutagenesis. BMC Biotechnol 15: 1–9. https://doi.org/10.1186/s12896-015-0162-8

Pujol N., S. Cypowyj, K. Ziegler, A. Millet, A. Astrain, *et al.*, 2008a Distinct innate immune responses to infection and wounding in the *C. elegans* epidermis. Curr Biol 18: 481–9. https://doi.org/10.1016/j.cub.2008.02.079.

Pujol N., O. Zugasti, D. Wong, C. Couillault, C. L. Kurz, *et al.*, 2008b Anti-fungal innate immunity in *C. elegans* is enhanced by evolutionary diversification of antimicrobial peptides. PLoS Pathog 4: e1000105. https://doi.org/10.1371/journal.ppat.1000105

Schwartz M. L., and E. M. Jorgensen, 2016 SapTrap, a Toolkit for High-Throughput CRISPR/Cas9 Gene Modification in *C. elegans*. Genetics 202: 1277–1288. https://doi.org/10.1534/genetics.115.184275

Serra N. D., C. B. Darwin, and M. V. Sundaram, 2023 *C. elegans* Hedgehog-related proteins are tissue- and substructure-specific components of the cuticle and pre-cuticle. 2023.12.26.573316.

Sun S., T. Theska, H. Witte, E. J. Ragsdale, and R. J. Sommer, 2022 The oscillating Mucin-type protein DPY-6 has a conserved role in nematode mouth and cuticle formation. Genetics 220: iyab233. https://doi.org/10.1093/genetics/iyab233

Taffoni C., S. Omi, C. Huber, S. Mailfert, M. Fallet, *et al.*, 2019 Microtubule plus-end dynamics link wound repair to the innate immune response. bioRxiv 512632. https://doi.org/10.1101/512632

Taffoni C., S. Omi, C. Huber, S. Mailfert, M. Fallet, *et al.*, 2020 Microtubule plus-end dynamics link wound repair to the innate immune response. Elife 9: e45047. https://doi.org/10.7554/eLife.45047

Thein M. C., G. McCormack, A. D. Winter, I. L. Johnstone, C. B. Shoemaker, *et al.*, 2003 *C. elegans* exoskeleton collagen COL-19: An adult-specific marker for collagen modification and assembly, and the analysis of organismal morphology. Developmental Dynamics 226: 523–539. https://doi.org/10.1002/dvdy.10259

Thomas P. D., D. Ebert, A. Muruganujan, T. Mushayahama, L.-P. Albou, *et al.*, 2022 PANTHER: Making genome-scale phylogenetics accessible to all. Protein Sci 31: 8–22. https://doi.org/10.1002/pro.4218

Zhang X., B. Harding, D. Aggad, D. Courtine, J. X. Chen, *et al.*, 2020 Antagonistic fungal enterotoxins intersect at multiple levels with host innate immune defences. bioRxiv 2020.11.23.391201. https://doi.org/10.1101/2020.11.23.391201

Ziegler K., C. L. Kurz, S. Cypowyj, C. Couillault, M. Pophillat, *et al.*, 2009 Antifungal innate immunity in *C. elegans*: PKCdelta links G protein signaling and a conserved p38 MAPK cascade. Cell Host Microbe 5: 341–52. https://doi.org/10.1016/j.chom.2009.03.006

Zugasti O., N. Bose, B. Squiban, J. Belougne, C. L. Kurz, *et al.*, 2014 Activation of a G protein-coupled receptor by its endogenous ligand triggers the innate immune response of *C. elegans*. Nat Immunol 15: 833–8. https://doi.org/10.1038/ni.2957

Zugasti O., N. Thakur, J. Belougne, B. Squiban, C. L. Kurz, *et al.*, 2016 A quantitative genome-wide RNAi screen in *C. elegans* for antifungal innate immunity genes. BMC Biol 14: 35. https://doi.org/10.1186/s12915-016-0256-3